PERGAMON Computers and Mathematics with Applications 45 (2003) 217–228

An International Journal
computers & mathematics
with applications

www.elsevier.com/locate/camwa

Asymmetric Responses of Rotating, Thin Disks Experiencing Large Deflections

A. C. J. Luo
Department of Mechanical and Industrial Engineering
Southern Illinois University Edwardsville
Edwardsville, IL 62034-1805, U.S.A.
aluo@siue.edu

C. D. Mote, Jr.
Office of the President, Main Administration Building
University of Maryland, College Park, MD 20742, U.S.A.
dmote@deans.umd.edu

Abstract—An analytical nonlinear solution for the asymmetric mode vibration of rotating disks is given in this paper through a recently developed, accurate plate theory instead of the von Karman model. The nonlinear solution can reduce to the linear one when nonlinear effects vanish. The symmetrical response is also recovered when the nodal diameter vanishes. The natural frequency varying with rotation speed and deflection amplitude is investigated through a 3.5-inch diameter computer memory disk. From this investigation, it is found that the softening of rotating disks may occur for larger nodal-diameter numbers. The methodology given in this paper can be applied to nonlinear responses in structures such as rotating shafts and traveling plates. © 2003 Elsevier Science Ltd. All rights reserved.

Keywords—Rotating disks, Nonlinear vibration, Softening disks, Hardening disks, Nonlinear differential equations.

1. INTRODUCTION

The vibration of rotating disks is a complicated, mathematical, and mechanical problem. With the wide application spectrum of rotating disks in industry, in 1850, Kirchhoff [1,2] developed the plate theory rather than the membrane theory, to investigate the free vibration of rotating disks. Lamb and Southwell [3] and Southwell [4] extended Kirchhoff analysis when rotational in-plane stresses in both free and centrally clamped disks were considered. Since then, the linear vibration analysis of rotating disks has been used to predict the response and stability of rotating disks (e.g., [5,6]). With computer developments, a thin, rotating circular disk is used as a primary data storage device. Increasing the rotation speed of disks leads to increases in data rates from memory. Therefore, rotation speeds of disks in disk drives are used to 25,000 rpm or higher. However, at such high speeds, rotating disk flatness and waviness become an important factor causing failures in data reliability, and the large amplitude vibration may happen. In the linear plate theory, membrane forces generated by disk deflections are not modeled, and it cannot give an appropriate prediction of the vibration of rotating disks in disk drives at such high speeds. The

0898-1221/03/$ - see front matter © 2003 Elsevier Science Ltd. All rights reserved. Typeset by AMS-TEX
PII: S0898-1221(02)00335-8

nonlinear plate theory has been considered as a candidate to investigate the vibration of rotating disks. For the nonlinear vibration of circular disks, in 1957, Tobias [7] applied the von Karman theory to the disk and reduced it to an oscillator problem with modes containing a specified number of nodal diameters through the Galerkin method. In 1964, Nowinski [8] used a similar method and theory to predict the natural frequencies of rotating disks, and the thermal stability of the rotating membrane disk was discussed [9]. The von Karman theory was also used for the nonlinear analysis of rotating disks (e.g., [10–12]). The von Karman theory considers a balance of force created by the curvature of the disks in the transverse direction. The membrane forces arising from force balances in the in-plane directions and moment balances are not included. The von Karman theory can give a good prediction of the symmetrical, transverse responses of rotating disks. To avoid the above limitations, in 1999, Luo [13] developed an approximate plate theory when the membrane forces in six force and moment balances were considered. Such a plate theory can apply to the asymmetrical responses of the rotating disks possessing flatness and waviness or experiencing an asymmetric response. For plate imperfections, in 1990, Wang [14] used the Monte Carlo method to analyze the nonlinear vibration of rectangular plates with random geometric imperfections. Herein, the disk imperfections caused by specific, nodal diameter waviness will be considered, instead of the random ones.

In this paper, nonlinear equations of motion governing the vibration of rotating disks with large deflection are derived from the accurate plate theory developed in [13]. Approximate, analytical solutions for the asymmetrical mode, nonlinear vibration of rotating disks are developed through the Galerkin method. The natural frequencies and displacements of the 3.5-inch diameter computer memory disk are considered as an example.

2. EQUATIONS OF MOTION

Consider a flexible, circular disk rotating with constant angular speed Ω, as sketched in Figure 1. The disk is clamped at the hub $r = a$, free at the outer edge $r = b$, and is of uniform thickness h. The rotating and stationary coordinate systems are (r, ϑ, τ) and (r, θ, τ), respectively. They satisfy

$$\theta = \vartheta + \Omega\tau. \tag{1}$$

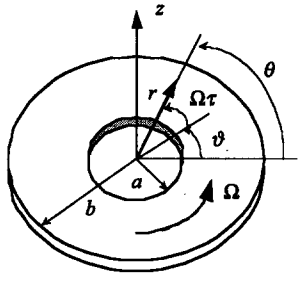

Figure 1. Asymmetric, rotating disk with clamped-free boundaries.

For large deflection plates, the accurate plate theory in [13] requires

$$\begin{aligned} &u_{r,r} \approx o(u_{\vartheta,r}) \approx o\left[(u_{z,r})^2\right], && u_{r,r} + \frac{1}{2}(u_{z,r})^2 \ll 1, \qquad 1 + \varepsilon_r \approx 1, \\ &\frac{1}{r}u_{r,\theta} \approx o\left(\frac{1}{r}u_{\theta,\theta}\right) \approx o\left[\left(\frac{1}{r}u_{z,\theta}\right)^2\right], && \frac{1}{r}u_{r,\theta} + \frac{1}{r}u_{\theta,\theta} + \frac{1}{2}\left(\frac{1}{r}u_{z,\theta}\right)^2 \ll 1, \qquad 1 + \varepsilon_\theta \approx 1, \end{aligned} \tag{2}$$

where a comma in the subscript denotes partial differentiation, and three displacement components of a material point on the disk are represented by u_r, u_θ, and u_z.

Under (2), three components of strain in the middle surface are approximated by

$$\varepsilon_r = u_{r,r} + \frac{1}{2}(u_{z,r})^2, \qquad \varepsilon_\theta = \frac{1}{r}u_r + \frac{1}{r}u_{\theta,\theta} + \frac{1}{2r^2}(u_{z,\theta})^2,$$
$$\gamma_{r\theta} = \frac{1}{r}u_{r,\theta} + u_{\theta,r} - \frac{1}{r}u_\theta + \frac{1}{r}(u_{z,r})(u_{z,\theta}). \tag{3}$$

From (2) and (3), the accurate plate theory in [13] gives force and moment balances

$$[N_r - (Q_r U_{z,r})]_{,r} + \frac{1}{r}[N_{r\theta} - (Q_\theta u_{z,r})]_{,\theta}$$
$$+ \frac{1}{r}(N_r - N_\theta) + \rho_0 h\Omega^2 r = \rho_0 h\left(\ddot{u}_r + 2\Omega\dot{u}_{r,\theta} + \Omega^2 u_{r,\theta\theta}\right), \tag{4}$$

$$\left[N_{r\theta} - \frac{1}{r}(Q_r u_{z,\theta})\right]_{,r} + \frac{1}{r}\left[N_\theta - \frac{1}{r}(Q_\theta u_{z,\theta})\right]_{,\theta} + \frac{2}{r}N_{r\theta} = \rho_0 h\left(\ddot{u}_\theta + 2\Omega\dot{u}_{\theta,\theta} + \Omega^2 u_{\theta,\theta\theta}\right), \tag{5}$$

$$\frac{1}{r}[r(N_r u_{z,r}) + (N_{r\theta}u_{z,\theta}) + rQ_r]_{,r} + \frac{1}{r}\left[\frac{1}{r}(N_\theta u_{z,\theta}) + (N_{r\theta}u_{z,r}) + Q_\theta\right]_{,\theta}$$
$$= \rho_0 h\left(\ddot{u}_z + 2\Omega\dot{u}_{z,\theta} + \Omega^2 u_{z,\theta\theta}\right), \tag{6}$$

$$M_{r,r} + \frac{1}{r}M_{r\theta,\theta} + \frac{1}{r}(M_r - M_\theta) + \frac{1}{r}(N_{r\theta}u_{z,\theta}) - Q_r = 0, \tag{7}$$

$$M_{r\theta,r} + \frac{1}{r}M_{\theta,\theta} + \frac{2}{r}(M_{r\theta}) + (N_{r\theta}u_{z,r}) - Q_\theta = 0, \tag{8}$$

where the superscript dot denotes derivative with respect to time τ, and $\{Q_r, Q_\theta\}$ denote shear forces. In the von Karman theory, shear force contributions in (4) and (5) and membrane force contribution in (7) and (8) were not considered. The membrane forces $\{N_r, N_\theta, N_{r\theta}\}$ are

$$N_r = \frac{Eh}{1-v^2}\left\{u_{r,r} + \frac{1}{2}(u_{z,r})^2 + v\left[\frac{1}{r}u_r + \frac{1}{r}u_{\theta,\theta} + \frac{1}{2r^2}(u_{z,\theta})^2\right]\right\},$$
$$N_\theta = \frac{Eh}{1-v^2}\left\{\frac{1}{r}u_r + \frac{1}{r}u_{\theta,\theta} + \frac{1}{2r^2}(u_{z,\theta})^2 + v\left[u_{r,r} + \frac{1}{2}(u_{z,r})^2\right]\right\}, \tag{9}$$
$$N_{r\theta} = \frac{Eh}{2(1+v)}\left[u_{\theta,r} + \frac{1}{r}u_{r,\theta} - \frac{1}{r}u_\theta + \frac{1}{r}(u_{z,r})(u_{z,\theta})\right],$$

and the bending and twisting moments $\{M_r, M_\theta, M_{r\theta}\}$ are

$$M_r = -D\left[u_{z,rr} + v\left(\frac{1}{r}u_{z,r} + \frac{1}{r^2}u_{z,\theta\theta}\right)\right],$$
$$M_\theta = -D\left(\frac{1}{r}u_{z,r} + \frac{1}{r^2}u_{z,\theta\theta} + vu_{z,rr}\right), \tag{10}$$
$$M_{r\theta} = -(1-v)D\left(\frac{1}{r}u_{z,r\theta} - \frac{1}{r^2}u_{z,\theta}\right),$$

where E and v are Young's modulus and Poisson ratio, and $D = Eh^3/12(1-v^2)$.

For convenience, we introduce dimensionless variables as follows:

$$R = \frac{r}{b}, \qquad U_R = \frac{u_r}{b}, \qquad U_\theta = \frac{u_\theta}{b}, \qquad U_z = \frac{u_z}{b}, \qquad \kappa = \frac{a}{b},$$
$$\varepsilon = \frac{h}{b}, \qquad t = \frac{\varepsilon c_p \tau}{\sqrt{12}\,b}, \qquad \Omega^* = \frac{\sqrt{12}\,b\Omega}{\varepsilon c_p}, \qquad c_p^2 = \frac{E}{\rho_0(1-v^2)}. \tag{11}$$

With (11), substitution of (7)–(10) into (4)–(6) yields

$$
\begin{aligned}
&U_{R,RR}+\frac{U_{R,R}}{R}-\frac{U_R}{R^2}+\frac{1-v}{2R^2}U_{R,\theta\theta}+\frac{1+v}{2R}U_{\theta,R\theta}-\frac{3-v}{2R^2}U_{\theta,\theta}\\
&+U_{Z,R}\left(U_{Z,RR}+\frac{1-v}{2R^2}U_{Z,\theta\theta}\right)+\frac{1+v}{2R^2}U_{Z,R\theta}U_{Z,\theta}+\frac{1-v}{2R}\left[(U_{Z,R})^2-\frac{1}{R^2}(U_{Z,\theta})^2\right]\\
&+\frac{\varepsilon^2}{12}\left\{\left[\left(\nabla^2U_R\right)_{,R}U_{Z,R}\right]_{,R}+\frac{1}{R^2}\left[\left(\nabla^2U_Z\right)_{,\theta}U_{Z,R}\right]_{,\theta}\right\}+\frac{\varepsilon^2}{12}\Omega^{*2}R\\
&=\frac{\varepsilon^2}{12}\left(\ddot{U}_R+2\Omega^*U_{R,\theta}+\Omega^{*2}U_{R,\theta\theta}\right),
\end{aligned}
\tag{12}
$$

$$
\begin{aligned}
&\frac{U_{\theta,\theta\theta}}{R^2}+\frac{1-v}{2}\left(U_{\theta,RR}+\frac{U_{\theta,R}}{R}-\frac{U_\theta}{R^2}\right)+\frac{1-v}{2R}U_{R,R\theta}+\frac{3-v}{2R^2}U_{R,\theta}\\
&+\frac{1+v}{2R}U_{Z,R}U_{Z,R\theta}+\frac{U_{Z,\theta}}{R}\left[\frac{U_{Z,\theta\theta}}{R^2}+\frac{1-v}{2}\left(U_{Z,RR}+\frac{U_{Z,R}}{R}\right)\right]\\
&+\frac{\varepsilon^2}{12}\left\{\left[\frac{1}{R}\left(\nabla^2U_Z\right)_{,R}U_{Z,\theta}\right]_{,R}+\frac{1}{R^3}\left[\left(\nabla^2U_Z\right)_{,\theta}U_{Z,\theta}\right]_{,\theta}\right\}\\
&=\frac{\varepsilon^2}{12}\left(\ddot{U}_\theta+2\Omega^*\dot{U}_{\theta,\theta}+\Omega^{*2}U_{\theta,\theta\theta}\right),
\end{aligned}
\tag{13}
$$

$$
\begin{aligned}
&\frac{1}{R}\left(R\left\{U_{R,R}+\frac{1}{2}(U_{Z,R})^2+v\left[\frac{U_R}{R}+\frac{U_{\theta,\theta}}{R}+\frac{1}{2R^2}(U_{Z,\theta})^2\right]\right\}U_{Z,R}\right.\\
&\left.+(1-v)\left\{U_{\theta,R}+\frac{U_{R,\theta}}{R}-\frac{U_\theta}{R}+\frac{1}{R}U_{Z,R}U_{Z,\theta}\right\}U_{Z,\theta}\right)_{,R}\\
&+\frac{1}{R}\left(\frac{1}{R}\left\{\frac{U_R}{R}+\frac{U_{\theta,\theta}}{R}+\frac{1}{2R^2}(U_{Z,\theta})^2+v\left[U_{R,R}+\frac{1}{2}(U_{Z,R})^2\right]\right\}U_{Z,\theta}\right.\\
&\left.+(1-v)\left\{U_{\theta,R}+\frac{U_{R,\theta}}{R}-\frac{U_\theta}{R}+\frac{1}{R}U_{Z,R}U_{Z,\theta}\right\}U_{Z,R}\right)_{,\theta}\\
&=\frac{\varepsilon^2}{12}\left(\nabla^4U_Z+\ddot{U}_Z+2\Omega^*\dot{U}_{Z,\theta}+\Omega^{*2}U_{Z,\theta\theta}\right).
\end{aligned}
\tag{14}
$$

Similarly, the membrane forces in (9) become

$$
\begin{aligned}
\bar{N}_R&=\left\{U_{R,R}+\frac{1}{2}(U_{Z,R})^2+v\left[\frac{1}{R}U_R+\frac{1}{R}U_{\theta,\theta}+\frac{1}{2R^2}(U_{Z,\theta})^2\right]\right\},\\
\bar{N}_\theta&=\left\{\frac{1}{R}U_r+\frac{1}{R}U_{\theta,\theta}+\frac{1}{2R^2}(U_{Z,\theta})^2+v\left[U_{R,R}+\frac{1}{2}(U_{Z,R})^2\right]\right\},\\
\bar{N}_{R\theta}&=\frac{(1-v)}{2}\left(U_{\theta,R}+\frac{1}{R}U_{R,\theta}-\frac{1}{R}U_\theta+\frac{1}{R}(U_{Z,R})(U_{Z,\theta})\right).
\end{aligned}
\tag{15}
$$

Accordingly, the boundary conditions become

$$
\begin{aligned}
&U_R=U_\theta=U_Z=0,\quad U_{Z,R}=0, && \text{at } R=\kappa,\\
&U_{Z,RR}+\mu\left(\frac{1}{R}U_{Z,R}+\frac{1}{R^2}U_{Z,\theta\theta}\right)=0, && \\
&\left(\nabla^2U_Z\right)_{,R}+\frac{1-v}{R^2}\left(U_{Z,R}-\frac{1}{R}U_Z\right)_{,\theta\theta}=0, && \text{at } R=1.
\end{aligned}
\tag{16}
$$

In addition, the radial and shear forces at $R=1$ require $\bar{N}_R=\bar{N}_{R\theta}=0$, i.e.,

$$
\begin{aligned}
&U_{R,R}+\frac{1}{2}(U_{Z,R})^2+v\left[\frac{1}{R}U_R+\frac{1}{R}U_{\theta,\theta}+\frac{1}{2R^2}(U_{Z,\theta})^2\right]=0,\\
&U_{\theta,R}+\frac{1}{R}U_{R,\theta}-\frac{1}{R}U_\theta+\frac{1}{R}(U_{Z,R})(U_{Z,\theta})=0,
\end{aligned}
\qquad \text{at } R=1. \tag{17}
$$

Considering the waviness only in the transverse direction, the initial conditions on transverse motion are

$$U_R = \dot{U}_R = U_\theta = \dot{U}_\theta = 0, \quad U_Z = \Phi(R,\theta), \quad \dot{U}_Z = \Psi(R,\theta), \qquad \text{at } t = 0. \tag{18}$$

3. PERTURBATION

To proceed with the perturbation analysis of (12)–(14) in small parameter $0 < \varepsilon = h/b \ll 1$, we consider series solutions satisfying (2) like

$$U_Z = \varepsilon U_Z^{(1)} + \varepsilon^3 U_Z^{(3)} + \cdots, \quad U_R = \varepsilon^2 U_R^{(2)} + \varepsilon^4 U_R^{(4)} + \cdots, \quad U_\theta = \varepsilon^2 U_\theta^{(2)} + \varepsilon^4 U_\theta^{(4)} + \cdots. \tag{19}$$

Without loss of generality, we retain terms through ε^2 to avoid higher order calculation. Substitution of (19) into (12),(13) for order ε^2 gives

$$\begin{aligned} &U_{R,RR}^{(2)} + \frac{U_{R,R}^{(2)}}{R} - \frac{U_R^{(2)}}{R^2} + \frac{1-v}{2R^2}U_{R,\theta\theta}^{(2)} + \frac{1+v}{2R}U_{\theta,\theta\theta}^{(2)} \\ &- \frac{3-v}{2R^2}U_{\theta,\theta}^{(2)} + U_{Z,R}^{(1)}\left(U_{Z,RR}^{(1)} + \frac{1-v}{2R^2}U_{Z,\theta\theta}^{(1)}\right) + \frac{1+v}{2R^2}U_{Z,R\theta}^{(1)}U_{Z,\theta}^{(1)} \\ &+ \frac{1-v}{2R}\left[\left(U_{Z,R}^{(1)}\right)^2 - \frac{1}{R^2}\left(U_{Z,\theta}^{(1)}\right)^2\right] + \frac{1}{12}\Omega^{*2}R = 0, \end{aligned} \tag{20}$$

$$\begin{aligned} &\frac{U_{\theta,\theta\theta}^{(2)}}{R^2} + \frac{1-v}{2}\left(U_{\theta,RR}^{(2)} + \frac{U_{\theta,R}^{(2)}}{R} - \frac{U_\theta^{(2)}}{R^2}\right) + \frac{1+v}{2R}U_{R,R\theta}^{(2)} + \frac{3-v}{2R^2}U_{R,\theta}^{(2)} \\ &+ \frac{1+v}{2R}U_{Z,R}^{(1)}U_{Z,R\theta}^{(1)} + \frac{U_{Z,\theta}^{(1)}}{R}\left[\frac{U_{Z,\theta\theta}^{(1)}}{R^2} + \frac{1-v}{2}\left(U_{Z,RR}^{(1)} + \frac{1}{R}U_{Z,R}^{(1)}\right)\right] = 0. \end{aligned} \tag{21}$$

The boundary conditions in (16) and (17) and initial conditions in (18) are retained for $U_R^{(2)}$, $U_\theta^{(2)}$, and $U_Z^{(1)}$,

$$\begin{aligned} &U_R^{(2)} = U_\theta^{(2)} = U_Z^{(1)} = 0, \quad U_{Z,R}^{(1)} = 0, && \text{at } R = \kappa; \\ &U_{Z,RR}^{(1)} + \mu\left(\frac{1}{R}U_{Z,R}^{(1)} + \frac{1}{R^2}U_{Z,\theta\theta}^{(1)}\right) = 0, \\ &\left(\nabla^2 U_Z^{(1)}\right)_{,R} + \frac{1-v}{R^2}\left(U_{,R}^{(1)} - \frac{1}{R}U_Z^{(1)}\right)_{,\theta\theta} = 0, && \text{at } R = 1, \end{aligned} \tag{22}$$

$$\begin{aligned} &U_{R,R}^{(2)} + \frac{1}{2}\left(U_{Z,R}^{(1)}\right)^2 + v\left[\frac{1}{R}U_R^{(2)} + \frac{1}{R}U_{\theta,\theta}^{(2)} + \frac{1}{2}\left(U_{Z,\theta}^{(1)}\right)^2\right] = 0, \\ &U_{\theta,R}^{(2)} + \frac{1}{R}U_{R,\theta}^{(2)} - \frac{1}{R}U_\theta^{(2)} + \frac{1}{R}U_{Z,R}^{(1)}U_{Z,\theta}^{(1)} = 0, \end{aligned} \qquad \text{at } R = 1, \tag{23}$$

$$U_R^{(2)} = \dot{U}_R^{(2)} = U_\theta^{(2)} = \dot{U}_\theta^{(2)} = 0, \quad U_Z^{(1)} = \Phi(R,\theta), \quad \dot{U}_Z^{(1)} = \Psi(R,\theta), \qquad \text{at } t = 0. \tag{24}$$

4. GALERKIN PROCEDURE

A solution for the transverse displacement satisfying the boundary condition (22) is

$$U_Z^{(1)} = \sum_{s=0}^{\infty}\sum_{m=0}^{4} C_m R^{m+s}\left[f_{sc}(t)\cos(s\theta) + f_{ss}(t)\sin(s\theta)\right], \tag{25}$$

where $f_{sc}(t)$ and $f_{ss}(t)$ are generalized coordinates. s denotes the number of nodal diameters, and the coefficients C_m $(m = 0, 1, \ldots, 4)$ are determined by (22) and (25). In this analysis, the

single-mode solutions for specified s will be sought. Solutions of mode coupling with many s will not be included.

Substitution of (25) into (20),(21) for specified s leads to

$$U_R^{(2)} = \Pi_0^{(2)}\left(f_{sc}^2 + f_{ss}^2\right) + \Pi_1^{(2)}\left[\cos(2s\theta)\left(f_{sc}^2 - f_{ss}^2\right) + 2\sin(2s\theta)(f_{sc}f_{ss})\right] - \frac{\Omega^{*2}}{96}\left\{R^3 + \frac{\left[(1+v)\kappa^4 - (3+v)\kappa^2\right]R^{-1}}{\left[(1-v)\kappa^2 + (1+v)\right]} + \frac{\left[(1-v)\kappa^4 + 3 + v\right]R}{\left[(1-v)\kappa^2 + (1+v)\right]}\right\}, \tag{26}$$

$$U_\theta^{(2)} = \Pi_2^{(2)}\left[\sin(2s\theta)\left(f_{sc}^2 - f_{ss}^2\right) - 2\cos(2s\theta)(f_{sc}f_{ss})\right], \tag{27}$$

and the functions $\Pi_0^{(2)}$, $\Pi_1^{(2)}$, and $\Pi_2^{(2)}$ are given by

$$\Pi_0^{(2)} = A_1^0 R + A_2^0 R^{-1} + \sum_{m_1,m_2=0}^{4}\left(\hat{A}_1^0\delta^2_{m_1+m_2+2s}R + \hat{A}_2^0\delta^0_{m_1+m_2+2s}R^{-1}\right)\log R + \sum_{m_1,m_2=0}^{4}\left[\hat{A}_1^0\frac{1-\delta^2_{m_1+m_2+2s}}{m_1+m_2+2s-2} + \hat{A}_2^0\frac{1-\delta^0_{m_1+m_2+2s}}{m_1+m_2+2s}\right]R^{m_1+m_2+2s-1}, \tag{28}$$

$$\begin{aligned}\Pi_1^{(2)} = {} & -a_1A_1R^{2s+1} - A_2R^{2s-1} + b_1A_3R^{-2s+1} + A_4R^{-2s-1} \\ & + \sum_{m_1,m_2=0}^{4}\left[-a_1\hat{A}_1\frac{1-\delta^2_{m_1+m_2}}{m_1+m_2-2} - \hat{A}_2\frac{1-\delta^0_{m_1+m_2}}{m_1+m_2}\right. \\ & \left. + b_1\hat{A}_3\frac{1-\delta^2_{m_1+m_2+4s}}{m_1+m_2+4s-2} + \hat{A}_4\frac{1-\delta^0_{m_1+m_2+4s}}{m_1+m_2+4s}\right]R^{m_1+m_2+2s-1} \\ & + \sum_{m_1,m_2=0}^{4}\left[-a_1\hat{A}_1\delta^2_{m_1+m_2}R^{2s+1} - \hat{A}_2\delta^0_{m_1+m_2}R^{2s-1}\right. \\ & \left. + b_1\hat{A}_3\delta^2_{m_1+m_2+4s}R^{-2s+1} + \hat{A}_4\delta^0_{m_1+m_2+4s}R^{-2s-1}\right]\log R,\end{aligned} \tag{29}$$

$$\begin{aligned}\Pi_2^{(2)} = {} & A_1R^{2s+1} + A_2R^{2s-1} + A_3R^{-2s+1} + A_4R^{-2s-1} \\ & + \sum_{m_1,m_2=0}^{4}\left[\hat{A}_1\frac{1-\delta^2_{m_1+m_2}}{m_1+m_2-2} + \hat{A}_2\frac{1-\delta^0_{m_1+m_2}}{m_1+m_2}\right. \\ & \left. + \hat{A}_3\frac{1-\delta^2_{m_1+m_2+4s}}{m_1+m_2+4s-2} + \hat{A}_4\frac{1-\delta^0_{m_1+m_2+4s}}{m_1+m_2+4s}\right]R^{m_1+m_2+2s-1} \\ & + \sum_{m_1,m_2=0}^{4}\left[\hat{A}_1\delta^2_{m_1+m_2}R^{2s+1} + \hat{A}_2\delta^0_{m_1+m_2}R^{2s-1}\right. \\ & \left. + \hat{A}_3\delta^2_{m_1+m_2+4s}R^{-2s+1} + \hat{A}_4\delta^0_{m_1+m_2+4s}R^{-2s-1}\right]\log R,\end{aligned} \tag{30}$$

where all the coefficients $A_1^0, A_2^0, \ldots, A_4$ and $\hat{A}_1^0, \hat{A}_2^0, \ldots, \hat{A}_4$ are determined by (20)–(23) and (26)–(30), and δ_i^j is the Kronecker delta. Substitution of (19) into (15), retention of the terms ε^2, and use of $U_R^{(2)}$ and $U_\theta^{(2)}$ gives the membrane forces

$$\begin{aligned}\bar{N}_R &= \frac{1}{96}\Omega^{*2}N_R^L + N_{R0}\left(f_{sc}^2 + f_{ss}^2\right) + N_{R1}\left[\left(f_{sc}^2 - f_{ss}^2\right)\cos(2s\theta) - 2(f_{sc}f_{ss})\sin(2s\theta)\right], \\ \bar{N}_\theta &= \frac{1}{96}\Omega^{*2}N_\theta^L + N_{\theta0}\left(f_{sc}^2 + f_{ss}^2\right) + N_{\theta1}\left[\left(f_{sc}^2 - f_{ss}^2\right)\cos(2s\theta) - 2(f_{sc}f_{ss})\sin(2s\theta)\right], \\ \bar{N}_{R\theta} &= N_{R\theta1}\left[\left(f_{sc}^2 - f_{ss}^2\right)\sin(2s\theta) + 2(f_{sc}f_{ss})\cos(2s\theta)\right],\end{aligned} \tag{31}$$

where $N_{R0}, R_{\theta 0}, \ldots, N_{R\theta 1}$ are computed through $\Pi_0^{(2)}$, $\Pi_1^{(2)}$, and $\Pi_2^{(2)}$. The linear membrane forces are

$$\begin{aligned} N_R^L &= \frac{(1-v)\left[(3+v)\kappa^2-(1+v)\kappa^4\right]}{\left[(1-v)\kappa^2+(1+v)\right]R^2}+\frac{(1+v)\left[(1-v)\kappa^4+3+v\right]}{(1-v)\kappa^2+(1+v)}-(3+v)R^2, \\ N_\theta^L &= \frac{(1-v)\left[(1+v)\kappa^4-(3+v)\kappa^2\right]}{\left[(1-v)\kappa^2+(1+v)\right]R^2}+\frac{(1+v)\left[(1-v)\kappa^4+3+v\right]}{(1-v)\kappa^2+(1+v)}-(3v+1)R^2. \end{aligned} \tag{32}$$

For specified s, substitution of (25)–(27) into (14) and use of the Galerkin method yields

$$\begin{aligned} &\ddot{f}_{sc}+2\Omega^* s\dot{f}_{ss}+\left(\frac{\alpha_s+\Omega^{*2}\gamma_0}{\beta_s}-\Omega^{*2}s^2\right)f_{sc}+\frac{\gamma_{sc}+\gamma_{s0}}{\beta_s}\left(f_{sc}^2+f_{ss}^2\right)f_{sc}=0, \\ &\ddot{f}_{ss}-2\Omega^* s\dot{f}_{sc}+\left(\frac{\alpha_s+\Omega^{*2}\gamma_0}{\beta_s}-\Omega^{*2}s^2\right)f_{ss}+\frac{\gamma_{sc}+\gamma_{s0}}{\beta_s}\left(f_{sc}^2+f_{ss}^2\right)f_{ss}=0, \end{aligned} \tag{33}$$

where the coefficients α_s, γ_0, β_s, γ_{s0}, γ_{sc} are related to the plate stiffness, centrifugal forces, inertia forces, and membrane forces. The second term in (33) is caused by the Coriolis force. When $s=0$, the two equations in (33) are identical. The problem reduces to the symmetrical one. For the symmetrical response, no Coriolis force contributes to the symmetrical response. Only the centrifugal force caused by rotation affects the symmetrical response. Therefore, the analyses given by Lamb and Southwell [3] and Southwell [4] are only for the symmetrical response of rotating disks.

The normalization of the initial conditions in (26) gives

$$\begin{aligned} f_{sc}^0 &= \frac{1}{\pi\Delta}\sum_{m=0}^{4}C_m\int_0^{2\pi}\int_\kappa^1\Phi(R,\theta)R^{m+s}\cos(s\theta)\,dR\,d\theta, \\ \dot{f}_{sc}^0 &= \frac{1}{\pi\Delta}\sum_{m=0}^{4}C_m\int_0^{2\pi}\int_\kappa^1\Psi(R,\theta)R^{m+s}\cos(s\theta)\,dR\,d\theta, \\ f_{ss}^0 &= \frac{1}{\pi\Delta}\sum_{m=0}^{4}C_m\int_0^{2\pi}\int_\kappa^1\Phi(R,\theta)R^{m+s}\sin(s\theta)\,dR\,d\theta, \\ \dot{f}_{ss}^0 &= \frac{1}{\pi\Delta}\sum_{m=0}^{4}C_m\int_0^{2\pi}\int_\kappa^1\Psi(R,\theta)R^{m+s}\sin(s\theta)\,dR\,d\theta, \end{aligned} \tag{34}$$

where

$$\Delta=\sum_{m=0}^{4}\sum_{n=0}^{4}\frac{1-\kappa^{m+n+2s+1}}{m+n+2s+1}C_mC_n. \tag{35}$$

5. NONLINEAR SOLUTIONS

Integration of (33) with initial conditions in (34) leads to a constant energy function

$$H=\frac{1}{2}\left(\dot{f}_{sc}^2+\dot{f}_{ss}^2\right)+\frac{1}{2}\left(\frac{\alpha_s+\Omega^*\gamma_0}{\beta_s}-(\Omega^* s)^2\right)\left(f_{sc}^2+f_{ss}^2\right)+\frac{\gamma_{sc}+\gamma_{s0}}{4\beta_s}\left(f_{sc}^2+f_{ss}^2\right)^2=E_0. \tag{36}$$

For the hardening disk $(\gamma_{sc}+\gamma_{s0})>0$, and for the softening disk $(\gamma_{sc}+\gamma_{s0})<0$. For $(\gamma_{sc}+\gamma_{s0})>0$, the solution to (33) with (34) is

$$\begin{aligned} f_{sc} &= \frac{\pi\hat{A}_s}{2k_sK(k_s)}\sum_{l=0}^{\infty}p_l\left(\cos\left\{\left[(2l+1)\omega_s+\Omega^* s\right]t+(2l+1)\varphi_0+\phi_0\right\}\right. \\ &\quad \left.+\cos\left\{\left[(2l+1)\omega_s-\Omega^* s\right]t+(2l+1)\varphi_0-\phi_0\right\}\right), \\ f_{ss} &= \frac{\pi\hat{A}_s}{2k_sK(k_s)}\sum_{l=0}^{\infty}p_l\left(\sin\left\{\left[(2l+1)\omega_s+\Omega^* s\right]t+(2l+1)\varphi_0+\phi_0\right\}\right. \\ &\quad \left.-\sin\left\{\left[(2l+1)\omega_s-\Omega^* s\right]t+(2l+1)\varphi_0-\phi_0\right\}\right), \end{aligned} \tag{37}$$

where $K(k_s)$ is the complete elliptic integral of the first kind, $k_s' = \sqrt{1-k_s^2}$, $\hat{A}_s$ is the amplitude, ω_s is the natural frequency without Coriolis forces, and φ_0 is the initial phase.

$$\begin{gathered}
\hat{A}_s = \frac{\sqrt{B-C}}{\sqrt{(\gamma_{sc}+\gamma_{s0})}}, \qquad k_s = \sqrt{\frac{1}{2}-\frac{C}{2B}}, \qquad \omega_s = \frac{\sqrt{B}\,\pi}{2\sqrt{B_s}\,K(k_s)}, \\
B = \sqrt{C^2+4(\gamma_{sc}+\gamma_{s0})\beta_s E_0}, \qquad C = \alpha_s + \Omega^{*2}\gamma, \qquad p_l = \operatorname{sech}\left[\left(l+\frac{1}{2}\right)\frac{\pi K(k_s')}{K(k_s)}\right], \\
\tan\phi_0 = \frac{f_{ss}^0}{f_{sc}^0}, \qquad \operatorname{tn}\left[\frac{2K(k_s)\varphi_0}{\pi}, k_s\right]\operatorname{dn}\left[\frac{2K(k_s)\varphi_0}{\pi}, k_s\right] = \frac{\pi\dot{A}_s^0}{2\omega_s K(k_s)A_s^0}, \\
A_s^0 = \sqrt{(f_{sc}^0)^2+(f_{ss}^0)^2}, \qquad \dot{A}_s^0 = \sqrt{\left[\dot{f}_{sc}^0-(\Omega^* s)f_{ss}^0\right]^2+\left[\dot{f}_{ss}^0+(\Omega^* s)f_{sc}^0\right]^2},
\end{gathered} \tag{38}$$

where dn and tn are the elliptic functions.

Substitution of (37) into (25) gives transverse displacement

$$\begin{aligned}
U_Z^{(1)} = \sum_{l=0}^{\infty}\sum_{m=0}^{4}\frac{\pi\hat{A}_s p_l C_m R^{m+s}}{2k_s K(k_s)}\,&(\cos\{[(2l+1)\omega_s+\Omega^* s]\,t+(2l+1)\varphi_0+\phi_0-s\theta\} \\
&+\cos\{[(2l+1)\omega_s-\Omega^* s]\,t+(2l+1)\varphi_0-\phi_0+s\theta\})\,.
\end{aligned} \tag{39}$$

For $(\gamma_{sc}+\gamma_{s0})<0$, the solution to (33) with (34) is

$$\begin{aligned}
f_{sc} = \frac{\pi\hat{A}_s}{2k_s K(k_s)}\sum_{l=0}^{\infty} q_l\,&(\sin\{[(2l+1)\omega_s+\Omega^* s]\,t+(2l+1)\varphi_0+\phi_0\} \\
&+\sin\{[(2l+1)\omega_s-\Omega^* s]\,t+(2l+1)\varphi_0-\phi_0\})\,, \\
f_{ss} = \frac{\pi\hat{A}_s}{2k_s K(k_s)}\sum_{l=0}^{\infty} q_l\,&(-\cos\{[(2l+1)\omega_s+\Omega^* s]\,t+(2l+1)\varphi_0+\phi_0\} \\
&+\cos\{[(2l+1)\omega_s-\Omega^* s]\,t+(2l+1)\varphi_0-\phi_0\})\,,
\end{aligned} \tag{40}$$

where

$$\begin{gathered}
\hat{A}_s = \sqrt{\frac{C_1-B_1}{|\gamma_{sc}+\gamma_{s0}|}}, \qquad k_s = \sqrt{\frac{C_1-B_1}{C_1+B_1}}, \qquad \omega_s = \frac{\sqrt{C_1+B_1}}{2\sqrt{2}}\frac{\pi}{K(k_s)}, \\
B_1 = \sqrt{C_1^2-4|\gamma_{sc}+\gamma_{s0}|\beta_s E_0}, \qquad C_1 = \alpha_s-\Omega^{*2}\gamma, \qquad q_l = \operatorname{csch}\left[\left(l+\frac{1}{2}\right)\frac{\pi K(k_s')}{K(k_s)}\right], \\
\tan\phi_0 = \frac{f_{ss}^0}{f_{sc}^0}, \qquad \operatorname{cs}\left[\frac{2K(k_s)\varphi_0}{\pi}, k_s\right]\operatorname{dn}\left[\frac{2K(k_s)\varphi_0}{\pi}, k_s\right] = \frac{\pi\dot{A}_s^0}{2\omega_s K(k_s)A_s}, \\
A_s = \sqrt{f_{sc}^2+f_{ss}^2}, \qquad \dot{A}_s^0 = \sqrt{\left[\dot{f}_{sc}^0-(\Omega^* s)f_{ss}^0\right]^2+\left[\dot{f}_{ss}^0+(\Omega^* s)f_{sc}^0\right]^2}.
\end{gathered} \tag{41}$$

Substitution of (40) into (25) gives

$$\begin{aligned}
U_Z^{(1)} = \sum_{l=0}^{\infty}\sum_{m=0}^{4}\frac{\pi A_s q_l C_m R^{m+s}}{2k_s K(k_s)}\,&(\sin\{[(2l+1)\omega_s+\Omega^* s]\,t+(2l+1)\varphi_0+\phi_0-s\theta\} \\
&+\sin\{[(2l+1)\omega_s-\Omega^* s]\,t+(2l+1)\varphi_0-\phi_0+s\theta\})\,;
\end{aligned} \tag{42}$$

$U_R^{(2)}$ and $U_\theta^{(2)}$ can be determined from (26) and (27) in a similar manner.

From time-dependent sine and cosine terms in (39) or (42), they indicate two dimensionless, modal frequencies

$$\omega_{1,2}^* = \begin{cases} (2l+1)\omega_s \pm \Omega^* s, & \text{if } (2l+1)\omega_s \geq \Omega^* s, \\ \Omega^* s \pm (2l+1)\omega_s, & \text{if } (2l+1)\omega_s \leq \Omega^* s. \end{cases} \tag{43}$$

When the nonlinear terms in (33) vanish, the linear solution is recovered

$$U_Z = \sum_{s=0}^{\infty} \sum_{m=0}^{4} C_m R^{m+s} \frac{\hat{A}_s}{2} \{\cos[(\omega_s + \Omega^* s)t + \varphi_0 + \phi_0 - s\theta] + \cos[(\omega_s - \Omega^* s)t + \varphi_0 - \phi_0 + s\theta]\}, \tag{44}$$

where

$$\omega_s = \sqrt{\frac{\alpha_s + \Omega^{*2}\gamma_0}{\beta_s}}, \qquad \hat{A}_s = \frac{\sqrt{\left(\dot{A}_s^0\right)^2 + \left(A_s^0\right)^2}}{\omega_s}, \qquad \tan\phi_0 = \frac{f_{ss}^0}{f_{sc}^0},$$
$$\tan\varphi_0 = \frac{\sqrt{\left[\dot{f}_{sc}^0 - (\Omega^* s) f_{ss}^0\right]^2 + \left[\dot{f}_{ss}^0 + (\Omega^* s) f_{sc}^0\right]^2}}{\omega_s \sqrt{f_{sc}^2 + f_{ss}^2}}. \tag{45}$$

Because $(\gamma_{sc} + \gamma_{s0}) = 0$ in (38) and (41), $k_s = 0$, $K(k_s) = \pi/2$, and ω_s in (45) is recovered. When $(\gamma_{sc} + \gamma_{s0}) = 0$, the subharmonic terms in (38) and (42) for $l \neq 0$ vanish. The linear solution in (44) is recovered.

6. ILLUSTRATIONS

Consider a 3.5-inch diameter disk similar to a digital memory disk with inner and outer radii of $a = 15.5\,\text{mm}$, $b = 43\,\text{mm}$; thickness $h = 0.775\,\text{mm}$, density $\rho_0 = 3641\,\text{kg/m}^3$, Young's modulus $E = 69\,\text{GPa}$, and Poisson's ratio $v = 0.33$. The natural frequencies from nondimensionalized $\omega_{1,2}^*$ are $\omega_{1,2} = \omega_{1,2}^* c_p \varepsilon / \sqrt{12}\, b$. For a comparison from (38) and (41), the natural frequency in the nonlinear analysis depends on A_s and nodal-diameter number s because E_0 and k_s depend on A_s and s.

As discussed in Section 4, for asymmetric mode responses of the rotating disk, the nodal diameter $s \neq 0$. For the asymmetric mode responses, the natural frequency varying with rotation speed and deflection amplitude is illustrated by solid curves through (12)–(14) and dashed curves

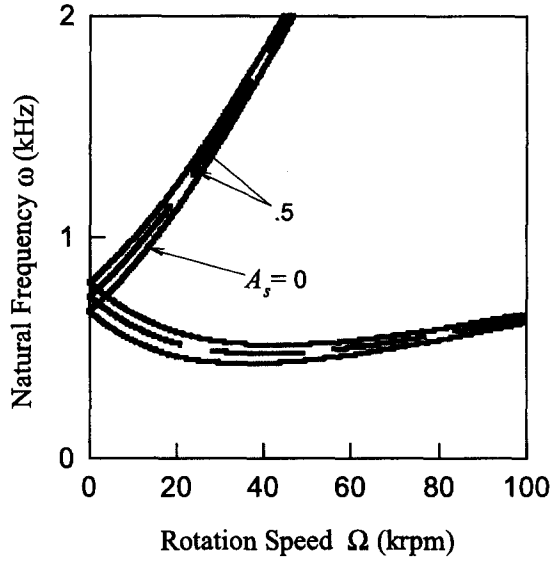

Figure 2. Natural frequency ($s = 1$, $A_s = 0, 0.5$). A_s is modal amplitude. The solid and dashed curves denote this theory and the von Karman theory. Two nonlinear models for $A_s = 0$ reduce to the linear model.

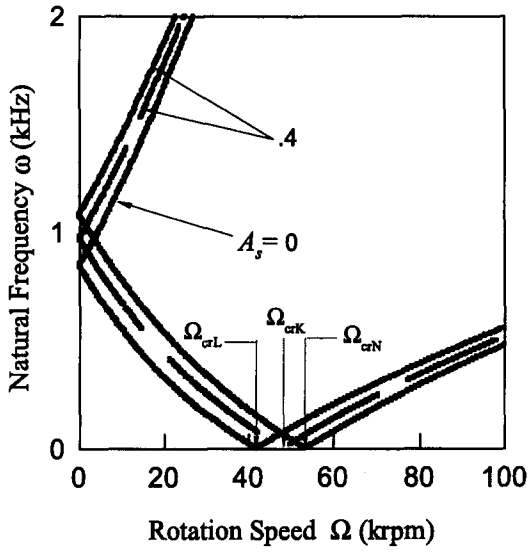

Figure 3. Natural frequency ($s = 2$, $A_s = 0, 0.4$). A_s is modal amplitude. The solid and dashed curves denote this theory and the von Karman theory. Two nonlinear models for $A_s = 0$ reduce to the linear model. Ω_{crL}, Ω_{crK}, and Ω_{crN} are the critical speeds predicted through the linear theory, the von Karman theory, and the new theory, respectively.

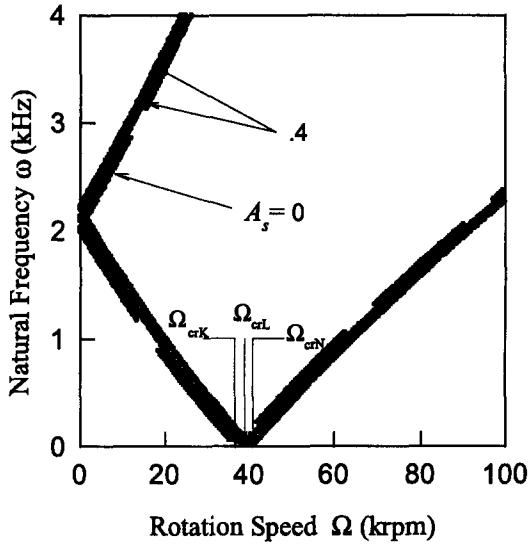

Figure 4. Natural frequency ($s = 4$, $A_s = 0, 0.4$) of the hardening disk. A_s is modal amplitude. The solid and dashed curves denote this theory and the von Karman theory. Two nonlinear models for $A_s = 0$ reduce to the linear model. Ω_{crL}, Ω_{crK}, and Ω_{crN} are the critical speeds predicted through the linear theory, the von Karman theory, and the new theory, respectively.

through the von Karman theory. When $A_s = 0.0$, the nonlinear results return to the linear ones. The natural frequency for an asymmetric mode response ($s = 1$) is plotted in Figure 2 when $A_s = 0, 0.5$ (or $|u_z| = 0, 0.241$ mm). For such an asymmetrical response, no critical speed exists. Note that the von Karman model results are obtained from the accurate model when the shear forces in (4) and (5) and the shear membrane forces in (7) and (8) vanish. Such changes reflect on the coefficient γ_{sc} in (33). When $s = 2$, the natural frequency for this asymmetric mode response is plotted in Figure 3. The critical speeds predicted through the linear theory, the von Karman theory, and the new theory are $\Omega_{crL} \approx 41.6$ krpm, $\Omega_{crK} \approx 47.8$ krpm, and $\Omega_{crN} \approx 53.2$ krpm at $A_s = 0.4$ (or $|\mu_z| \approx 0.138$ mm), respectively.

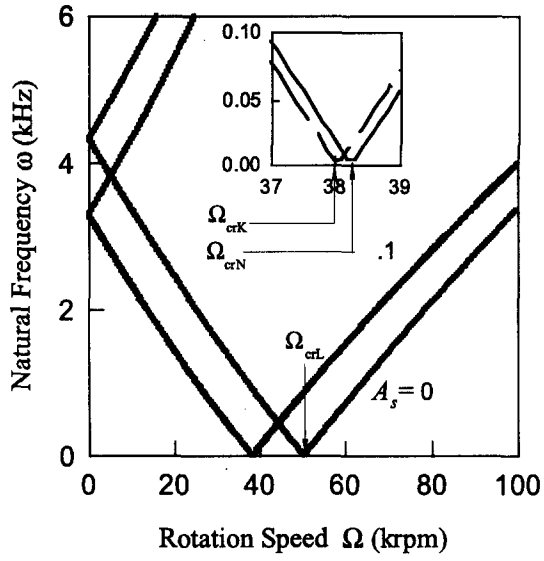

Figure 5. Natural frequency ($s = 6$, $A_s = 0, 0.1$). A_s is modal amplitude. The solid and dashed curves denote this theory and the von Karman theory. Two nonlinear models for $A_s = 0$ reduce to the linear model. Ω_{crL}, Ω_{crK}, and Ω_{crN} are the critical speeds predicted through the linear theory, the von Karman theory, and the new theory, respectively.

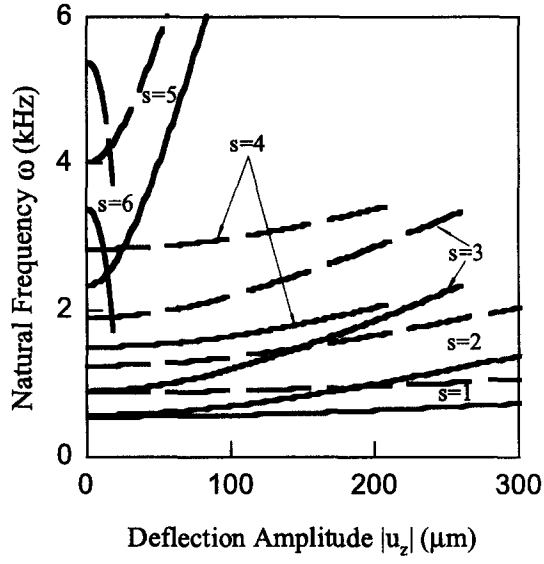

Figure 6. Natural frequency versus deflection amplitude by use of the accurate nonlinear model ($\Omega = 10$ krpm). A_s is modal amplitude. The nonlinear model for $A_s = 0$ reduces to the linear model. The solid and dashed curves give the frequency for the backward and forward wave responses.

For $s = 4$, the natural frequency of the rotating disk for $A_s = 0.4$ ($|u_z| \approx 0.082$ mm) is illustrated in Figure 4. The von Karman theory shows that the rotating disk used in disk drives becomes softening. The new plate theory shows that such a rotating disk is still like a hardening spring. The three predictions of critical speeds are $\Omega_{crL} \approx 38.6$ krpm, $\Omega_{crK} \approx 36.8$ krpm, and $\Omega_{crN} \approx 40.2$ krpm at $A_s = 0.4$, respectively. The von Karman theory gives the critical speed less than the linear plate theory. The natural frequency for $s = 6$ is plotted in Figure 5. From the two nonlinear theories, the rotating disk for this asymmetric response becomes softening. The critical speeds given by the three plate theories are $\Omega_{crL} \approx 50.2$ krpm, $\Omega_{crK} \approx 30.6$ krpm, and $\Omega_{crN} \approx 31.0$ krpm at $A_s = 0.1$ ($|u_z| = 0.015$ mm), respectively. The two nonlinear critical speeds

are less than the linear one (i.e., at $A_s = 0$). When the disk becomes softening, its vibration can be easily induced.

For illustration of deflection effects, the natural frequency varying with dimensional deflection amplitudes is plotted for $\Omega = 10$ krpm in Figure 6. The solid and dashed curves give the frequency for the backward and forward traveling waves. The rotating disk is hardening for $s = 1, 2, \ldots, 5$. Thus, the natural frequency increases when the deflection amplitude increases. However, for $s = 6$, the rotating disk becomes softening, and the natural frequency decreases with increasing the deflection amplitude. It is observed that the sensitivity of the natural frequency to the deflection amplitude increases with increasing nodal diameters.

7. CONCLUSIONS

The responses of the asymmetric mode vibration of rotating disks with initial waviness are investigated through a recently developed, accurate plate theory instead of the von Karman one. The nonlinear solutions of rotating disks reduce to the linear ones when the nonlinear effects vanish. The asymmetric results reduce to the symmetric ones when $s = 0$. Such a methodology presented in this paper can be applied to nonlinear responses in structures such as rotating shafts, traveling plates, and shells.

REFERENCES

1. G. Kirchhoff, Über das Gleichgewicht und die Bewegung einer elastischen Scheibe, *Journal für die Reine und Angewandte Mathematik* **40**, 51–88, (1850).
2. G. Kirchhoff, Ueber die Schwingungen einer kreisformigen elastischen Scheibe, *Poggendorffs Annal* **81**, 258–264, (1850).
3. H. Lamb and R.V. Southwell, The vibrations of a spinning disc, *Proceedings of Royal Society of London* **99**, 272–280, (1921).
4. R.V. Southwell, On the free transverse vibrations of a uniform circular disc clamped at its centre, and on the effects of rotation, *Proceedings of Royal Society of London* **101**, 133–153, (1922).
5. C.D. Mote, Jr., Free vibration of initially stressed circular plates, *Journal of Engineering for Industry* **87**, 258–264; (1965).
6. W.D. Iwan and T.L. Moeller, The stability of a spinning elastic disk with a transverse load system, *Journal of Applied Mechanics* **43**, 485–490, (1976).
7. S.A. Tobias, Free undamped nonlinear vibrations of imperfect circular disks, *Proceedings of the Institute of Mechanical Engineers* **171**, 691–701, (1957).
8. J.L. Nowinski, Nonlinear transverse vibrations of a spinning disk, *Journal of Applied Mechanics* **31**, 72–78, (1964).
9. J.L. Nowinski, Stability of nonlinear thermoelastic waves in membrane-like spinning disks, *Journal of Thermal Sciences* **4**, 1–11, (1981).
10. S.H. Advani, Stationary waves in a thin spinning disk, *International Journal of Mechanical Sciences* **9**, 307–313, (1967).
11. S.H. Advani and P.Z. Bulkeley, Nonlinear transverse vibrations and waves in spinning membrane discs, *International Journal of Non-Linear Mechanics* **4**, 123–127, (1969).
12. A.A. Renshaw and C.D. Mote, Jr., A perturbation solution for the flexible rotating disk: Nonlinear equilibrium and stability under transverse loading, *Journal of Sound and Vibration* **183**, 309–326, (1995).
13. A.C.J. Luo, An approximate theory for geometrically-nonlinear thin plates, *International Journal of Solids and Structures* **37**, 7655–7670, (2000).
14. F.Y. Wang, Monte Carlo analysis of nonlinear vibration of rectangular plates with random geometric imperfections, *International Journal of Solids and Structures* **26** (1), 99–110, (1990).